Study on Debonding Failure Load of RC Beams Strengthened with FRP Sheets

Zhishen Wu *, Hedong Niu **

*Dr. of Eng., Assoc. Prof., Dept. of Urban & Civil Eng., Ibaraki Univ., Nakanarusawa-cho 4-12-1, Hitachi Ibaraki 316-8511
**Dr. Cand. of Eng., Dept. of Urban & Civil Eng., Ibaraki Univ., Nakanarusawa-cho 4-12-1, Hitachi Ibaraki 316-8511

The load-carrying capacities and stiffnesses of concrete structures can be enhanced by the application of FRP sheets, but the failure of these systems may be due to some local failure, such as debonding along the FRP-concrete interface initiated from the end of a flexural or shear crack of concrete. This study focuses on developing a methodology for predicting the debonding failure load due to flexural cracks based on the fracture energy criterion. Based on the theoretical derivations, a quantitative criterion governing the debonding failure for the retrofitted beams is established by adopting the solution from the simple shear test. Moreover, an iterative analytical method is developed to predict the response of strengthened beams based on the strain compatibility. Through application of the proposed method to the existing experimental results, it is clarified that the debonding failure mode is governed by interfacial fracture energy and its value ranged normally from 0.38 to 1.22N/mm excluding several special cases, which can be used for the design and the performance evaluation of the FRP-strengthened concrete structures.

Key Words: *FRP composites, Local failure, Debonding failure, Analytical model, Interfacial fracture energy, Design equation*

1. Introduction

Fiber Reinforced Plastics (FRP) has considerable potential in the rehabilitation and retrofitting of existing civil infrastructures. Considerable research has been directed to investigate the applications of FRP as external reinforcement primarily for strengthening the concrete structures. The load-carrying capacities and stiffnesses can be enhanced with externally bonded FRP sheets; however, different types of failure modes, which may limit these gains, have been reported [1][2][3][4]. It is observed that the debonding failure initiated from the end of flexural cracks of concrete, generally occurring in the concrete substrate, is a typical failure mode for the strengthened beams with FRP sheets. Therefore, there poses an urgent need for rational evaluating or predicting the structural capacity due to this type of failure mode.

Many researchers paid much attention to the premature failure at the cut-off point of the FRP plate and gave many theoretical derivations for interfacial shear stress to predict the failure load according to a variety of strength-based theories [5][6][7][8][9][10]. However, there are few studies concerned with the debonding failure initiated from the flexural cracks near the maximum moment. The debonding mechanism is a local failure process driven by stress intensities associated with stress transfer between the concrete and the FRP sheets. The traditional strength-based theory can only predict the initial debonding load but not the ultimate debonding failure load.

This paper focuses on the development of an analytical method on how to predict the debonding failure load due to flexural cracks based on the fracture energy criterion. First, on the basis of the theoretical derivation, the bond and stress transfer behavior and debonding mechanism along the FRP-concrete interface around flexural cracks in a FRP-strengthened beam is regarded to be similar to that of the simple shear test, such as a single-lap shear test. Therefore, the experimental results and the solutions based on the simple shear test can be used for the case of FRP-strengthened beams as fundamental experimental data. Due to these considerations, an energy-based failure criterion for typical debonding failure of the FRP-strengthened beams is proposed. Then, an iterative analytical method is developed to predict the response of a strengthened beam based on the

strain compatibility. Finally, the interfacial fracture energy consumed for debonding failure is identified through applying the proposed method to the existing available experiments.

2. Basic Theory

2.1 Shear Transfer in FRP-strengthened Beams with Flexural Cracks

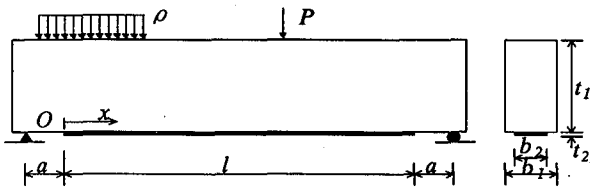

Fig. 1 Simply supported beam strengthened with FRP

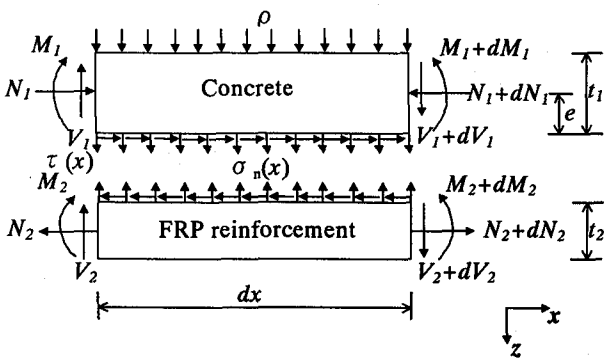

Fig. 2 Forces in infinitesimal element of FRP-strengthened concrete beam

A differential section dx, can be cut out from the FRP-strengthened concrete beam as shown in Fig. 2. The composite beam is made from three materials: concrete (or RC concrete), adhesive layer and FRP reinforcement. In the present analysis, linear elastic behavior is regarded to be for all the materials; the adhesive is assumed to only play a role in transferring the stresses from the concrete to the FRP reinforcement and the stresses in the adhesive layer do not change through the direction of the thickness.

The strains in the concrete near the adhesive interface and the external FRP reinforcement can be expressed as, respectively:

$$\varepsilon_1(x)=\frac{du_1(x)}{dx}=\frac{M_1(x)}{E_1W_1}-\frac{N_1(x)}{E_1A_1} \tag{1}$$

$$\varepsilon_2(x)=\frac{du_2(x)}{dx}=\frac{N_2(x)}{E_2A_2}-\frac{M_2(x)}{E_2W_2} \tag{2}$$

And by adopting the equilibrium conditions of the concrete (or RC concrete), we have:

x-direction: $$\frac{dN_1(x)}{dx}=\tau(x)b_2 \tag{3}$$

z-direction: $$\frac{dV_1(x)}{dx}=-\left[\sigma_n(x)b_2+\rho b_1\right] \tag{4}$$

moment equilibrium: $$\frac{dM_1(x)}{dx}=V_1(x)-\tau(x)b_2e \tag{5}$$

The equilibrium of the external FRP reinforcement in the x-, z- direction and moment equilibrium can be also written as:

x-direction: $$\frac{dN_2(x)}{dx}=\tau(x)b_2 \tag{6}$$

z-direction: $$\frac{dV_2(x)}{dx}=\sigma_n(x)b_2 \tag{7}$$

moment equilibrium:

$$\frac{dM_2(x)}{dx}=V_2(x)-\tau(x)b_2t_2/2 \tag{8}$$

Considering that the bending stiffness of the FRP sheets is far less than that of the concrete beam to be strengthened, the bending moment in the FRP sheets can be neglected for simplicity in the derivation of shear stress. The FRP sheets can thus be assumed to only carry the tension stress and transfer the shear stress to the surrounding concrete through the adhesive layer. On the basis of the work done by Täljsten [10] where the author only focused on the cut-off point of the plate and did not take any concrete crack or failure model into consideration, the interfacial shear stress near the flexural crack is derived in what follows.

The shear stress in the adhesive can be expressed as follows:

$$\tau(x)=K_s\left[u_2(x)-u_1(x)\right] \tag{9}$$

where $K_s=\frac{G_a}{s}$, G_a and s are shear modulus and thickness of the adhesive, respectively; $u_1(x)$ and $u_2(x)$ are the horizontal displacements of the concrete and the FRP reinforcement, respectively, at the adhesive interface.

Differentiating equation (9) twice and combining equation (1), (2), (3), (5) and (6) gives:

$$\frac{d^2\tau(x)}{dx^2}-\alpha^2\tau(x)+\frac{K_s}{E_1W_1}V_1(x)=0 \tag{10}$$

where $\alpha^2=K_sb_2\left[\frac{1}{E_2A_2}+\frac{1}{E_1A_1}+\frac{e}{E_1W_1}\right]$, E_2,A_2,b_2 are elastic modulus, section area and width of FRP reinforcement, respectively, E_1,A_1 are elastic modulus and section area of concrete, respectively, $W_1=\frac{I_1}{e}$, I_1 is the moment of inertia of transformed section based on concrete for the R/C beam to be strengthened and e the distance from the neutral axis to the bottom of the R/C beam; $V_1(x)$ is the shear force at section x due to externally applied

loads since the shear force is neglected in the external FRP reinforcement and here it is assumed that the expression of $V_1(x)$ is a linear function of x for the convenience of solution;

The solution to equation (10) is given by:

$$\tau(x) = C_1 \cosh(\alpha x) + C_2 \sinh(\alpha x) + \frac{K_s}{\alpha^2 E_1 W_1} \cdot V_1(x) \qquad (11)$$

where C_1, C_2 are the constants of integration to be determined by the boundary conditions.

Based on the above equation, the authors investigated the effect of the flexural cracks around the maximum moment on interfacial shear stress transfer for several load cases: three-point bending beam, four-point bending beam and distributed loading beam. The results of the solutions were compared to numerical results by a finite element analysis. It is concluded that the gradient of the moment, or shear force has an insignificant effect on the distribution of interfacial shear stress after concrete cracks, the interfacial shear stress between the flexural cracks is mainly provided by the axial stress difference in FRP, and there is high shear stress concentrations around flexural cracks which may lead to interfacial fracture. In addition, the normal stress near the flexural cracks does not show high concentration like that at the cut-off point [8]. Here take three point-bending beam as an example to explain the solution as shown in Fig. 3.

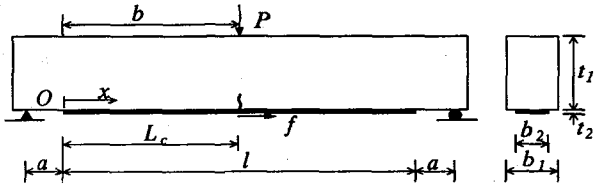

Fig. 3 Three-point bending beam with a flexural crack

The interfacial shear stress for three point-bending beam shown in Fig. 3 can be obtained from equation (11):

$$\tau(x) = \frac{K_s P(l+a-b)}{\alpha E_1 W_1 (l+2a)} \left\{ a \left[\frac{(\cosh(\alpha L_c) - 1)\cosh(\alpha x)}{\sinh(\alpha L_c)} - \sinh(\alpha x) \right] + \frac{1}{\alpha} - \frac{L_c \cosh(\alpha x)}{\sinh(\alpha L_c)} \right\} + \frac{\alpha f \cosh(\alpha x)}{b_2 \sinh(\alpha L_c)}$$

$$x \in [0,\ L_c],\quad L_c \le b \qquad (12)$$

where a, b, l, L_c, P are defined in Fig. 3; f is the axial force in FRP at the flexural crack.

Generally, the maximum shear stress in adhesive layer near the flexural cracks around the maximum moment ignoring the minor terms can be obtained from the following approximate equation (see also in [9]):

$$\tau_{\max} = \sqrt{\frac{G_a}{s E_2 t_2}} \frac{f}{b_2} \qquad (13)$$

This approximate expression may be used to predict the initial debonding load based on the failure criterion, which is defined by:

$$|\tau_{\max}| < \tau_f \qquad (14)$$

where τ_f is the local shear strength of the adhesive interface and can be determined by the simple pull-out test of bonded FRP.

A notched strengthened beam with FRP [1] is used to verify the correctness of the derived equation (12) as shown in Fig. 4 and the material properties are given in Table 1.

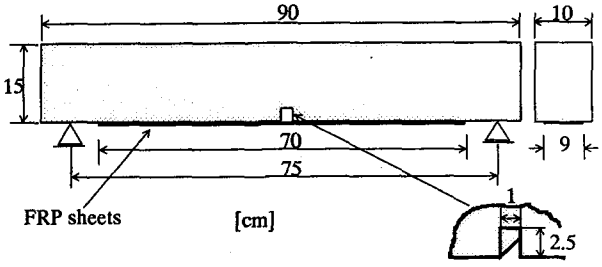

Fig. 4 Details of the specimen used in the verification

Table 1 Material properties for the studied specimen

concrete	Young's modulus [GPa]	30
	compressive strength [MPa]	39.2
	Poisson's ratio	0.16
	slump [cm]	8.0
CFRP sheets	Young's modulus [GPa]	235
	tensile strength [GPa]	3.2
	thichness [mm]	0.11
	Poisson's ratio	0.3
epoxy	Young's modulus [GPa]	3.43
	Poisson's ratio	0.35

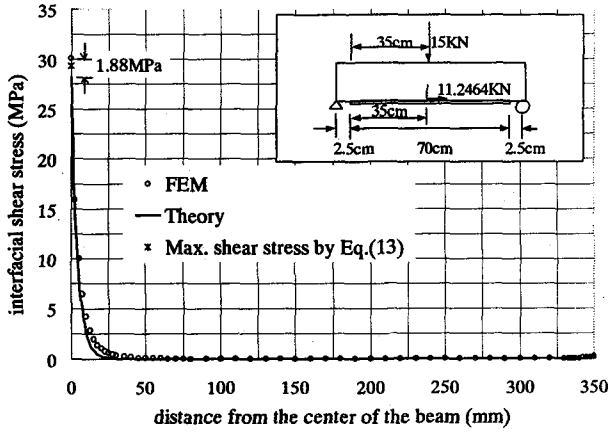

Fig. 5 Interfacial shear stress distribution near the crack

The comparison of the theoretical derivation with the "ABAQUS" finite element analysis is illustrated in Fig. 5. Although there are deviations between the two results, the overall prediction is in a relative good agreement.

Moreover, the authors found that the effective transfer length of interfacial shear stresses and the load-carrying capacity also increase with increasing elastic modulus E_2 and thickness t_2 of FRP.

2.2 Theory on Simple Shear Test

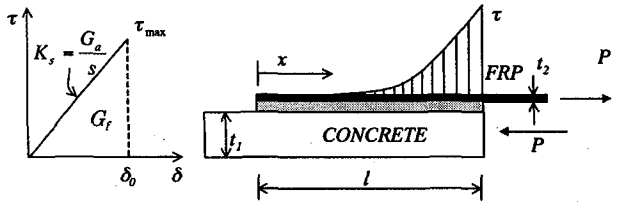

(a) (b)

Fig. 6 (a) Linear shear stress-slip relationship; (b) Shear stress transfer in a simple shear test.

Täljsten [12] applied a linear and nonlinear fracture mechanics to the plate bonding technique and derived a series of formulae based on linear shear stress-slip relationship and linear elastic assumption of the materials (Fig. 6 (a)). The derived expression for the interfacial shear stress can be written as:

$$\tau(x) = \frac{P\varpi}{b_2}\frac{\cosh(\varpi x)}{\sinh(\varpi l)}, \quad 0 \le x \le l \tag{15}$$

where l is the bonding length; $\varpi^2 = \frac{G_a}{s}\left(\frac{1}{E_1 t_1} + \frac{1}{E_2 t_2}\right)$,

$E_1 t_1$ and $E_2 t_2$ are the stiffness for concrete and FRP respectively; other symbols are defined as before.

A graphic representation of the shear stress distribution is shown in Fig. 6(b). The shear stress at the end where the force is introduced can be obtained from equation (15) as:

$$\tau(l) = \sqrt{\frac{G_a}{sE_2 t_2}}\frac{P}{b_2}, \ (l \text{ is sufficiently large}) \tag{16}$$

Through comparing equation (16) with equation (13) and ignoring the influence of compressive normal stresses along the FRP-concrete interface due to flexural deflection of the composite beams, it can be found that the shear stress transfer near the flexural cracks in the FRP strengthened beams is similar to that in the simple shear test. So some analytical/experimental results based on simple shear test of bonded FRP may be applied in investigating the debonding behavior of the composite beams due to flexural cracks.

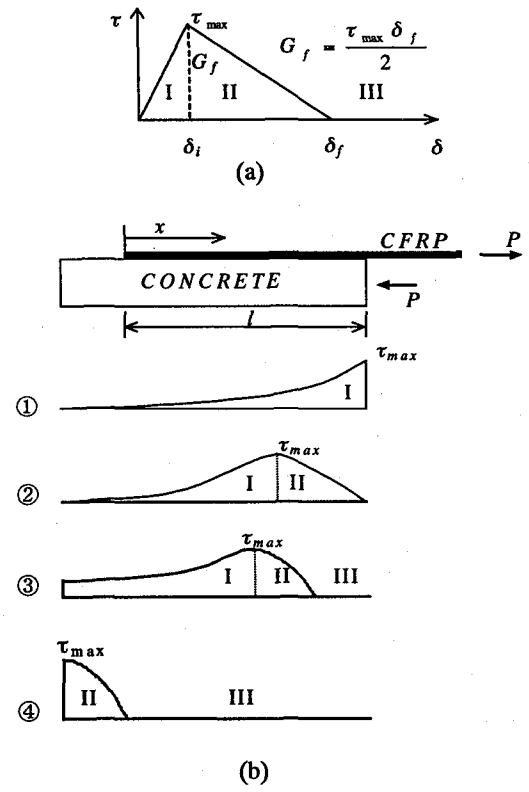

Fig. 7 (a) Bilinear shear stress-slip relationship; (b) Shear transfer for different stages in a simple shear test [13].

Using the bilinear relationship of $\tau - \delta$ (as shown in Fig. 7(a)), on the other hand, Brosens and Van Gemert [13] derived the expression for determining the maximum load in function of the bonding length like:

$$P(l) = \frac{E_2 A_2 \lambda\omega\delta_f \sin[\lambda\omega(l - x_p)]}{1 + m_2\gamma_2} \tag{17}$$

where $\lambda = \sqrt{\frac{\delta_i}{\delta_f - \delta_i}}$; $\omega = \sqrt{\frac{\tau_{max}(1 + m_2\gamma_2)}{\delta_i E_2 h_2}}$;

$\tan(\omega x_p) = \lambda \tan[\lambda\omega(l - x_p)]$; $m_2 = \frac{E_2}{E_1}$ and $\gamma_2 = \frac{A_2}{A_1}$.

The problem in the above equations is that x_p is defined as an implicit function and can only be obtained by iteration. The shear stress transfer for different stages is illustrated in Fig. 7(b).

Provided that the bonding length is larger than the effective bond length, the equations for determining the maximum load in both liner and bilinear stress-slip relationship can be expressed in the same form only differing in the definition of the fracture energy G_f:

$$P_{\max} = b_2\sqrt{2G_f E_2 t_2} \tag{18}$$

where E_2, t_2 and b_2 are elastic modulus, thickness and width of FRP, respectively; G_f is the area of the $\tau - \delta$ curve for the linear relationship illustrated in Fig. 6(a) or the area of the complete $\tau - \delta$ curve for the bilinear relationship illustrated in Fig. 7(a).

3. Analytical Method to Predict the Response of Composite Beams

3.1 Analytical Model

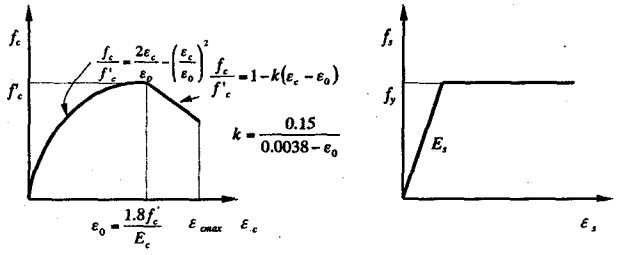

(a) concrete (b) steel

Fig. 8 Constitutive relationship for materials

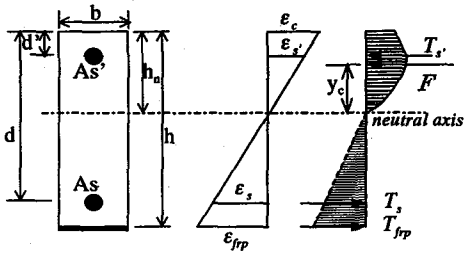

Fig. 9 Analytical model based on strain compatibility

In the analysis presented in this section, the following assumptions are made:

(a) Linear strain distribution throughout the full depth of the section;

(b) No slip between the longitudinal reinforcing steel and the surrounding concrete;

(c) No slip between the external FRP reinforcement and the base of the concrete beam above;

(d) No premature FRP separation or shear failure is accounted for, composite action is maintained up to failure;

(e) The tensile strength of the adhesive is ignored.

To simulating the real response of the FRP strengthened concrete beam accurately, the nonlinear constitutive relationships for concrete and steel reinforcement in the composite beam is used in the analysis (as shown in Fig. 8). The FRP composites are assumed to behave linear elastic to failure. Here, the ultimate strain of the concrete is regarded as 0.0035 [4].

The calculation of the concrete compression force must be performed by integrating the nonlinear concrete stress distributed over the compressed area. Based on the force equilibrium of the section, the neutral axis location h_n can be calculated from the following equations.

Case 1. The maximum concrete compressive strain is less than the threshold ε_0

$$Ah_n^3 + Bh_n^2 + Ch_n + D = 0 \tag{19}$$

Considering that the steel reinforcement does not reach its yielding strength gives:

$$A = f'_c b\varepsilon_{frp}^2 + 3\varepsilon_0 f'_c b\varepsilon_{frp} - 1.5\psi E_c \varepsilon_0^2 b\varepsilon_{frp}$$

$$B = 3\varepsilon_0\left[E_{frp}A_{frp}\varepsilon_0 - f'_c bh + E_s\left(A_s + A'_s\right)\varepsilon_0 + 1.5\psi E_c bh\varepsilon_0\right]\varepsilon_{frp}$$

$$C = -3\varepsilon_0^2\left[2E_{frp}A_{frp}h + E_s\left[(h+d')A'_s + (h+d)A_s\right] + 1.5\psi E_c bh^2\right]\varepsilon_{frp}$$

$$D = 3\varepsilon_0^2\left[E_{frp}A_{frp}h^2 + E_s\left(A'_s hd' + A_s hd\right) + 0.5\psi E_c bh^3\right]\varepsilon_{frp}$$

Considering that the lower steel reinforcement reaches its yielding strength gives:

$$A = f'_c b\varepsilon_{frp}^2 + 3\varepsilon_0 f'_c b\varepsilon_{frp} - 1.5\psi E_c \varepsilon_0^2 b\varepsilon_{frp}$$

$$B = 3\varepsilon_0\left(E_{frp}A_{frp}\varepsilon_0 - f'_c bh + E_s A'_s\varepsilon_0 + f_y A_s\varepsilon_0 + 1.5\psi E_c bh\varepsilon_0\right)\varepsilon_{frp}$$

$$C = -3\varepsilon_0^2\left[2E_{frp}A_{frp}h + E_s\left(h+d'\right)A'_s + 2f_y A_s h + 1.5\psi E_c bh^2\right]\varepsilon_{frp}$$

$$D = 3\varepsilon_0^2\left(E_{frp}A_{frp}h^2 + E_s A'_s hd' + f_y A_s h^2 + 0.5\psi E_c bh^3\right)\varepsilon_{frp}$$

The moment of compression zone to the neutral axis can be given by:

$$M_{compression} = f'_c bh_n^2\left[\frac{2h_n}{3\varepsilon_0(h-h_n)} - \frac{h_n^2\varepsilon_{frp}}{4\varepsilon_0^2(h-h_n)^2}\right]\varepsilon_{frp} + \frac{E_s A'_s\left(h_n - d'\right)^2\varepsilon_{frp}}{h-h_n} \tag{20}$$

Case 2. The maximum concrete compressive strain is larger than the threshold ε_0

$$Ah_n^2 + Bh_n + C = 0 \tag{21}$$

Considering that the steel reinforcement does not reach its yielding strength gives:

$$A = f'_c b\varepsilon_0 + 1.5kf'_c b\varepsilon_0^2 + 3(1+k\varepsilon_0)f'_c b\varepsilon_{frp} + 1.5\left(kf'_c b + \psi E_c b\right)\varepsilon_{frp}^2$$

$$B = -\left\{f'_c bh\varepsilon_0(2+3k\varepsilon_0) + 3f'_c bh(1+k\varepsilon_0)\varepsilon_{frp} + 3\left[E_{frp}A_{frp} + E_s\left(A_s + A'_s\right) + \psi E_c bh\right]\varepsilon_{frp}^2\right\}$$

$$C = f_c' b\varepsilon_0 h^2(1+1.5k\varepsilon_0)+3\left[E_{frp}A_{frp}h+E_s(A_s'd'+A_sd)+0.5E_cbh^2\right]\varepsilon_{frp}^2$$

Considering that the lower steel reinforcement reaches its yielding strength gives:

$$A = f_c' b\varepsilon_0 + 1.5kf_c' b\varepsilon_0^2 + 3(1+k\varepsilon_0)f_c' b\varepsilon_{frp} + 1.5(kf_c' b+\psi E_c b)\varepsilon_{frp}^2$$

$$B = -\left[f_c' bh\varepsilon_0(2+3k\varepsilon_0)+3f_c' bh(1+k\varepsilon_0)\varepsilon_{frp}+3f_yA_s\varepsilon_{frp}+3(E_{frp}A_{frp}+E_sA_s'+\psi E_cbh)\varepsilon_{frp}^2\right]$$

$$C = f_c' b\varepsilon_0 h^2(1+1.5k\varepsilon_0)+3f_yA_sh\varepsilon_{frp}+3\left(E_{frp}A_{frp}h+E_sA_s'd'+0.5E_cbh^2\right)\varepsilon_{frp}^2$$

The moment of compression zone to the neutral axis can be given by:

$$M_{compression} = \frac{f_c' b(h-h_n)^2}{\varepsilon_{frp}^2}\left\{\frac{5\varepsilon_0^2}{12}+\frac{1}{2}(1+k\varepsilon_0)\cdot\left[\left(\frac{h_n\varepsilon_{frp}}{h-h_n}\right)^2-\varepsilon_0^2\right]-\frac{k}{3}\left[\left(\frac{h_n\varepsilon_{frp}}{h-h_n}\right)^3-\varepsilon_0^3\right]\right\}+\frac{E_sA_s'(h_n-d')^2\varepsilon_{frp}}{h-h_n} \quad (22)$$

The compression force of the section which equals to the tension force can be written as:

$$F = E_{frp}A_{frp}\varepsilon_{frp}+\frac{E_sA_s(d-h_n)\varepsilon_{frp}}{h-h_n}+\frac{\psi E_cb(h-h_n)\varepsilon_{frp}}{2} \quad (23)$$

where the second term should be changed to f_yA_s when the lower steel reinforcement reaches its yielding strength.

So the applied location of the integrated compression force can be given by:

$$y_c = \frac{M_{compression}}{F} \quad (24)$$

The moment equilibrium of the section leads to:

$$E_{frp}A_{frp}(h-h_n+y_c)\varepsilon_{frp}+\frac{E_sA_s(d-h_n)(d-h_n+y_c)}{h-h_n}\cdot\varepsilon_{frp}+\psi E_cb(h-h_n)\left[y_c+\frac{2(h-h_n)}{3}\right]\frac{\varepsilon_{frp}}{2} = M(x) \quad (25)$$

where the second term at the left hand should be changed to $f_yA_s(d-h_n+y_c)$ when the lower steel reinforcement reaches its yielding strength; $M(x)$ is the bending moment of the composite beam at x .

In the above equations, ψ is a parameter denoting whether or not concrete carries tension force (0-- cracked section analysis; 1-- uncracked section analysis).

When the stress or strain in the FRP is known, it is simple to use the above equations to calculate the load. While making the opposite operation, an iterative procedure is employed to locate the neutral axis position and calculate the stress or strain in the FRP. In the analysis, it is assumed that failure is reached when either the concrete strain or the FRP reaches the corresponding ultimate strain.

To verify the accuracy of the analytical model presented here, the comparisons with experimental results are made in the following section.

3.2 Verification of the Aforementioned Method

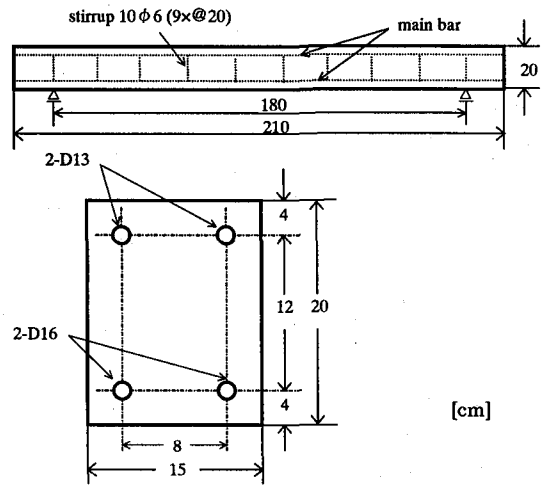

Fig. 10 Details of specimen [2]

Table 2 Material properties

concrete	Young's modulus [GPa]	25.4, 31.5
	compressive strength [MPa]	30.2, 34.6
	Poisson's ratio	0.16
	slump [cm]	9.0, 10.5
CFRP sheets	Young's modulus [GPa]	230
	tensile strength [GPa]	3.2
	thickness [mm]	0.111
	Poisson's ratio	0.3
steel	Young's modulus [GPa]	210
	Yielding strength [MPa]	420
epoxy	Young's modulus [GPa]	3.43
	Poisson's ratio	0.35

To investigate the different reinforcement effects for various RC beams with different ratios of flexural and shear capacities and structural optimization of reinforcement, a series of experiments have been conducted by Wu et al. [2]. The experimental program consists of three-point bending tests on the FRP-strengthened beams with or without stirrups and FRP end reinforcement. The details of the specimens are shown in Fig. 10.

During the experiment, the load and the corresponding strain distribution in FRP were recorded in detail. To verify

Table 3. The theoretical values versus the experimental results [2]

Specimen types / Items	RC_1 (Without stirrups)	RCS_1 (With stirrups)	RCS_S1 (With stirrups and FRP end reinforcement)
Concrete compressive strength (MPa)	30.2	34.6	34.6
Layer number	1	2	2
Measured strain at the center span ($\mu\varepsilon$)	8091	6580	9995
Experimental Load (KN)	65.0	72.2	82.1
Theoretical calculation load (KN)	63.0	70.4	79.2
Error (%)	3.1	2.5	3.5

the correctness of the aforementioned analytical method, the calculation values based on the experimental results of strain values of FRP sheets are compared to the experimental data as shown in Table 3. It is shown that RC flexural beam theory can be used to predict the response of the composite beam, even in the case of existing a certain extent of debonding.

4. An Energy-based Criterion for Predicting Debonding Failure Load

Niu and Wu [11] pointed out that the bond strength is mainly responsible for the initiation of debonding fracture and the propagation of debonding is governed by the interfacial fracture energy through a numerical simulation with nonlinear fracture mechanics. Based on the aforementioned conclusion that the shear stress transfer near the flexural crack in a FRP-strengthened beam is similar to that of simple shear test and the theory on simple shear test, it is assumed that the interfacial fracture energy consumed for ultimate debonding failure should be a characteristic material parameter concerned with interfacial behavior along FRP-concrete interface, concrete strength and debonding position. When the flexural crack occurs in the concrete, a high shear stress concentration will be induced and subsequently an interfacial crack will be initiated. Whether the interfacial crack propagates or not is mainly dependent on the fracture energy. Once the crack propagates to a certain distance, an unstable propagation may be occurred and then the ultimate debonding failure will be resulted in.

Generally, it is observed that many flexural cracks are distributed along the FRP-strengthened beams before the occurrence of the debonding failure studied in this paper and the occurrence and propagation of interfacial debonding is initiated from the maximum moment location.

As stated above, the axial force in FRP around the maximum moment can be easily obtained by equation (18) if the interfacial fracture energy for ultimate debonding failure is obtained from a simple shear test, and then the debonding failure load can be predicted based on the RC flexural beam theory presented in the section 3.

5. Identification of the Fracture Energy from the Available Experiments

Considering that the quantification of interfacial fracture energy for debonding failure in a FRP-strengthened beam cannot be found in the literatures at present, the identification of the interfacial fracture energy is conducted in this section using the proposed method and the available experimental results.

According to the simple shear tests of bonded FRP sheets reported by Wu et al. [14] and Nishida et al. [15], the experimental results and the identified interfacial fracture energy for the case of debonding failure specimens or strain energy release rate for the case of FRP rupture specimens calculated based on equation (18) are summarized in Table 4 and Table 5, respectively. It can be found that the identified interfacial fracture energy for debonding failure is ranged from 0.45 to 2.5N/mm.

To the best of the authors' knowledge, the failure load is often lower than or equal to the debonding failure load in the case of the failure mode due to rupture of FRP. This phenomenon can be easily explained by the interfacial fracture energy-based concept proposed by the authors. The failure mode can be transferred from rupture of FRP to debonding failure only dependent on whether the maximum strain energy release rate is lower or not than the interfacial fracture energy for debonding failure, that is to say, the structural system may fail in rupture of FRP if the maximum strain energy release rate cannot reach the interfacial fracture energy for debonding failure, or fail in debonding failure if the strain energy release rate is lager than the interfacial fracture energy.

According to [13], Brosens and Van Gemert found that there is a linear relationship between the interfacial fracture energy and the concrete strength based on a large number of experiments. Due to some disturbance factors such as uncertainties of bond condition and material strength etc., this conclusion cannot be drawn from Table 5.

Table 4 Summary of the pure shear test [14]

Specimens No.	Failure load (kN)	Bond area (cm^2)	Identified interfacial fracture energy or strain energy release rate (N/mm)	Failure mode
1	15.4	150.0	0.51	Debonding failure
2	21.0	200.0	0.94	Debonding failure
3	18.6	164.0 【150.0】	0.73	Debonding failure
4	20.1	182.5 【150.0】	0.86	Debonding failure
5	17.5	207.7 【150.0】	0.65	Rupture of FRP
6	25.6	214 【200.0】	1.39	Debonding failure
7	28.1	232.5 【200.0】	1.68	Debonding failure
8	34.1	257.7 【200.0】	2.47	Debonding failure
9	27.3	150.0	1.59	Debonding failure
10	19.3	150.0	0.79	Debonding failure

* Values in the parentheses are the bond area ignoring the additional area caused by the FRP end anchorage (after [14])

Table 5 Summary of the uniaxial pull-out test [15]

Experimental parameters	Specimen name	Concrete strength (MPa)	Properties of sheets				Max. load (KN)	Failure mode	Identified fracture energy or strain energy release rate (N/mm)
			type	Width (mm)	Thick. (mm)	Elastic modulus (GPa)			
Base	Base	34.9	Carbon	30	0.111	266.3	13.57	Debonding	0.865
Concrete strength	FC53.4	53.4	Carbon	30	0.111	266.3	17.45	Rupture	1.431
	FC75.5	75.5	Carbon	30	0.111	266.3	15.36	Debonding	1.109
Width of Sheet	B10	34.9	Carbon	10	0.111	266.3	6.25	Rupture	1.652
	B50	38.8	Carbon	50	0.111	266.3	22.30	Rupture	0.851
	B70	41.5	Carbon	70	0.111	266.3	29.84	Debonding	0.768
	B90	41.5	Carbon	90	0.111	266.3	29.44	Debonding	0.452
Sheet	Aramid	36.5	Aramid	30	0.169	85.5	14.70	Debonding	2.077
Impregnated with resin	Low elasticity	42.4	Carbon	30	0.111	250.6	12.72	Rupture	0.808

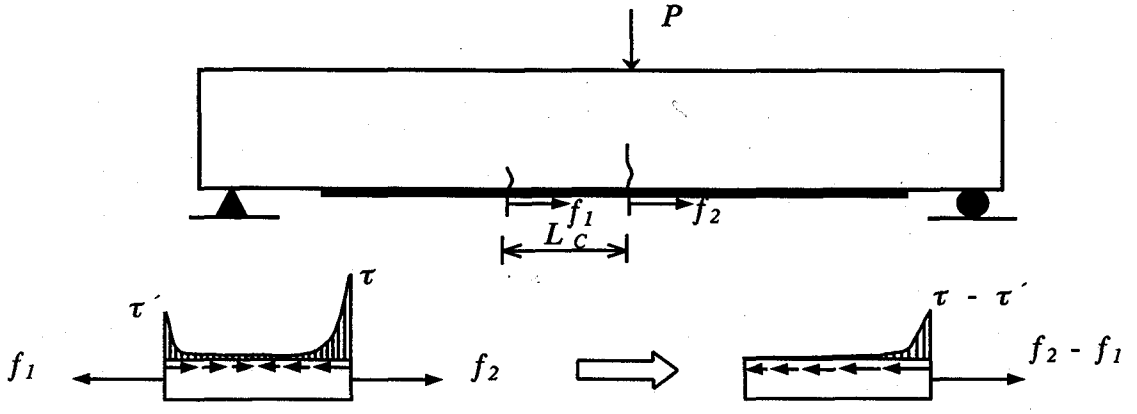

Fig. 11 The actual axial force of FRP used during identifying the interfacial fracture energy for debonding failure

Considering that there are often many distributed flexural cracks along the FRP-strengthened beams before occurrence of debonding failure, the shear stress transfer between the two flexural cracks is illustrated in Fig. 11. Here we adopt a calculation model as shown in Fig. 11 to approximate the shear transfer of the simple shear test in identifying the interfacial fracture energy for debonding failure of the FRP-strengthened beams.

Through applying the proposed method to the existing available experiments of RC beams strengthened with FRP [2][3][16][17][18], the interfacial fracture energy consumed for the case of debonding failure or the maximum strain energy release rate for the case of FRP rupture along FRP-concrete interface is identified in Table 6, where the effect of

Table 6 Identification of the interfacial fracture energy consumed for debonding failure*

Ref.	Specimen types	Concrete comp. strength (MPa)	Properties of FRP					Max. moment (KN·m)	Failure load (KN)	Identified fracture energy or strain energy release rate (N/mm)	Failure mode
			Layer number	Width (cm)	E_{FRP} (GPa)	Thickness per layer (mm)	Reinforcement stiffness (E_{FRP}·t_{FRP}) (GPa·mm)				
[2]	RC_1	30.2	1	14	230	0.111	25.53	30.6	65.0	0.643	Deb.
	RC_2	30.2	1	14	230	0.111	25.53	31.1	68.9	0.803	Deb.
	RCS_1	34.6	2	14	230	0.111	51.06	33.1	73.5	0.676	Deb.
	RCS_S1	34.6	2	14	230	0.111	51.06	38.3	85.0	1.219	Deb.
	Beam without FRP prestressing	43.5	2	14	230	0.111	51.06	37.0	82.3	1.131	Deb.
[3]	BCB-SC	31.4	1	14	230	0.111	25.53	33.7	112.32	0.523	Rup.
	BCB-SCB	31.4	1	14	230	0.111	25.53	34.1	113.80	0.665	Rup.
	BC-SC/S	31.4	1	14	230	0.111	25.53	35.8	119.39	0.893	Rup.
	BC2B-SCB/S	31.4	2	14	230	0.111	51.06	40.4	134.79	1.243	Rup.
	BC3B-SC/S	31.4	3	14	230	0.111	76.59	44.3	147.74	1.684	Deb.
	BC3B-SC/S	31.4	3	14	230	0.111	76.59	47.3	157.74	≥1.684**	Deb.
[16]	No.2	31.3	1	14	230	0.167	38.41	33.9	67.7	0.381	Deb.
	No.3	31.3	1	14	230	0.167	38.41	30.7	76.7	0.465	Deb.
	No.4	31.3	1	14	230	0.167	38.41	30.5	87.0	0.587	Deb.
	No.6	39.0	2	14	230	0.167	76.82	39.3	78.6	0.547	Deb.
	No.7	39.0	3	14	230	0.167	115.23	42.8	85.6	0.736	Deb.
	No.8	39.0	1	14	230	0.167	38.41	37.0	74.9	0.477	Deb.
[17]	A-70	23.93	1	8	126.51	0.286	36.18	29.9	39.81	0.573	Rup.
	A-140	23.93	1	8	126.51	0.286	36.18	30.2	40.21	≥0.573**	Deb.
	C-70	23.93	1	8	230.46	0.167	38.49	28.2	37.56	0.447	Rup.
	C-140	23.93	1	8	230.46	0.167	38.49	31.1	41.48	0.447	Rup.
	CT-140	23.93	1	8	230.46	0.248	57.15	32.8	43.74	0.695	Deb.
[18]	Plate-2	42.5	1	10	127.5	1.2	153	54.5	121.0	2.873	Deb.
	Plate-4	42.5	1	10	127.5	0.6	76.5	45.1	100.2	1.736	Deb.

* The identified values are calculated on the corresponding L_e which is taken as the distance between two flexural cracks as shown in Fig. 11;

**These value are calculated for the maximum theoretical load and the actual value should be equal or larger one.

reinforcement stiffness (E_{FRP}·t_{FRP}) on the effective transfer length of shear stress is taken into account by taking L_e according to the reinforcement stiffness as $L_e = 15 + 5 \times (\frac{E_{FRP} t_{FRP}}{25.53} - 1)$.

As seen from Table 6, the following regularities can be obtained:

(1) For the similar reinforcement stiffness, the values of interfacial fracture energy for debonding failure can be localized in a small range.

(2) Based on the study of the specimens in [3][17], it is found that whether the maximum strain energy release rate reaches the critical interfacial fracture energy consumed for debonding failure or not governs the final failure mode. Rupture of FRP is mainly due to that the maximum strain energy release rate cannot reach the interfacial fracture energy for debonding failure. For the case of rupture of FRP sheets, it is regarded that the identified value should be less than the interfacial fracture energy for debonding failure.

(3) A very interesting phenomenon can be found in [17] when comparing A-70 specimen with A-140 specimen that the two specimens appear different failure modes at attaining the interfacial fracture energy for debonding failure, which is also observed in some other experiments [1]. This is because that the load-carrying capacities due to the FRP debonding and FRP rupture are quite close.

(4) The effect of concrete strength appears no regularity from Table 4~Table 6. As a conclusion, the interfacial fracture energy value is theoretically related only to the concrete interfacial strength according to [13] if the bond fracture normally propagates through the concrete adjacent to the interface, but actually it may be also related to the interfacial strength of epoxy layer or the interfacial strength between epoxy layer and concrete within which debonding occurs due to the imperfection of bonding process in the experiments. In addition, the reinforcement stiffness of FRP may also affect the debonding position and state of the interfacial concrete.

(5) The interfacial fracture energy ranges from 0.38 to 1.22N/mm excluding several special cases such as the strengthened beams with FRP plate (two specimens in [18]), and FRP end reinforcement or anchorage (BC2B-SCB/S, BC3B'-SC/S and BC3B-

SC/S in [3]).

6. Conclusions

Based on the previous works of many researchers, debonding failure due to flexural cracks around the maximum moment along the FRP-strengthened beam is investigated in detail. From the analysis presented herein, the following conclusions can be drawn:

(1) For the first time, an energy-based criterion for predicting debonding failure of the FRP-strengthened beams is proposed based on the theoretical derivations and the available experiments.

(2) An iterative analytical method is developed to predict the response of the composite beams based on the strain compatibility, which is verified by comparison of the analytical calculations with the experiments.

(3) Through analysis on the available experiments, the fracture energy for debonding failure is identified and it is found that the value ranged normally from 0.38 to 1.22N/mm which to some extent, depends on the reinforcement stiffness.

(4) Based on the proposed method, it is found that the failure mode can be transferred from debonding failure to rupture of FRP when the maximum strain energy release rate cannot reach the critical value for debonding failure.

(5) The energy-based criterion for predicting debonding failure proposed in the paper is of great value to the design and the performance evaluation of FRP-strengthened concrete structures.

In this paper, the effect of the deflection of the composite beams on the interfacial debonding due to compressive normal stresses along the FRP-concrete interface is ignored, which may increase the interfacial fracture energy and should be studied in the future.

References

1) Wu, Z. S., Matsuzaki, T. and Tanabe, K., "Experimental study on fracture mechanism of FRP-reinforced concrete beams", Symposium on Non-Metallic (FRP) Reinforcement for Concrete Structures, Japan Concrete Institute, May, 1998, pp.119-126 (In Japanese)

2) Wu, Z. S., Matsuzaki, T., Fukuzawa, K. and Kanda, T., "Strengthening effects on RC beams with externally prestressed carbon fiber sheets", Journal of Materials, Concrete Structures and Pavements, JSCE, 2000, pp.??-?? (to be appeared, in Japanese)

3) Ichikawa, M. and Wu, Z. S., "Experimental study on flexural and shear behavior of RC beams strengthened with FRP sheets", Proceedings of the Japan Concrete Institute, Vol. 20, No. 1, 1998, pp.449-454 (In Japanese)

4) Quantrill, R. J., Hollaway, L. C., and Thorne, A. M., "Experimental and analytical investigation of FRP strengthened beam response: Part I", Magazine of Concrete Research, Vol. 48, No. 177, December, 1996, pp.331-342

5) Roberts, T. M., "Approximate analysis of shear and normal stress concentrations in the adhesive layer of plated RC beams", The Structural Engineer, vol. 67, No. 12, 20 June, 1989, pp.229-233

6) Ziraba, Y. N., Baluch, M. H., Basunbul, I. A., Sharif, A. M., Azad, A. K., and Al-Sulaimani, G. J., "Guidelines toward the design of reinforced concrete beams with external plates", Vol. 91, No. 6, November-December, 1994, pp.639-646

7) Quantrill, R. J., Hollaway, L. C., and Thorne, A. M., "Predictions of the maximum plate end stresses of FRP strengthened beams: Part II", Magazine of Concrete Research, Vol. 48, No. 177, December, 1996, pp.343-351

8) Malek, A. M., Saadatmanesh, H., and Ehsani, M. R., "Prediction of failure load of R/C beams strengthened with FRP plate due to stress concentration at the plate end", ACI Structural Journal, Vol. 95, No. 1, January-February, 1998, pp.142-152

9) Saadatmanesh, H. and Malek, A. M., "Design guidelines for flexural strengthening of RC beams with FRP plates", Journal of composites for construction, Vol. 2, No. 4, November, 1998, pp.158-164

10) Täljsten, B., "Strengthening of beams by plate bonding", Journal of materials in civil engineering, Vol. 9, No. 4, November, 1997, pp.206-212

11) Niu, H. D., Wu, Z. S., and Asakura, T., "A numerical analysis on bonding mechanism of FRP-strengthened concrete structures using nonlinear fracture mechanics", Proceedings of the Japan Concrete Institute, Vol. 21, No. 3, 1999, pp.73-78

12) Täljsten, B., "Strengthening of concrete prism using the plate-bonding technique", International Journal of Fracture Mechanics 82, 1996, pp.253-266

13) Brosens, K. and Van Gemert, D., "Plate end shear design for external CFRP laminates", Fracture Mechanics of Concrete Structures, Proceedings FRAMCOS-3, AEDIFICATIO Publishers, D-79104 Freiburg, Germany, 1998, pp.1793-1804

14) Wu, Z. S., Murayama, D., and Yoshizawa, H., "An experiment study on bonding behavior and its improvement approach of CFRP sheets in anchorage zone", Proceedings of the Japan Concrete Institute, Vol. 21, No. 2, 1999, pp.211-216 (In Japanese)

15) Nishida, H., Kamiharako, A., Shimomura, T. and Maruyama, K., "Bond mechanism between continuous fiber and concrete", Proceedings of the Japan Concrete Institute, Vol. 21, No. 3, 1999, pp.1507-1512 (In Japanese)

16) Takeo, K., Matsushita, H., Sagawa, Y. and Ushigome, T., "Experiment of RC beam reinforced with CFRP adhesive method having variety of shear-span ratio", Proceedings of the Japan Concrete Institute, Vol. 21, No. 2, 1999, pp.205-210 (In Japanese)

17) Mikami, H., Kishi, N., Sato, M. and Kurihashi, Y. "Effect strengthened area on bonding capacity of RC beams adhered with FRP sheet", Proceedings of the Japan Concrete Institute, Vol. 21, No. 3, 1999, pp.1549-1545 (In Japanese)

18) Kurokawa, T., Wu, Z. S. and Yoshizawa, H., "Experimental study on the crack characteristics of RC beam strengthened with CFRP plate", Proceedings of the 54th annual conference of the Japan society of civil engineers, 5, September, 1999, pp.702-703 (In Japanese)

(Received September 17, 1999)